Performance of diamond-like carbon-protected rubber under cyclic friction

Martinez-Martinez, D.; van der Pal, J. P. ; Pei, Y. T.; de Hosson, J. Th. M.

Published in:
Journal of Applied Physics

DOI:
10.1063/1.3665445

Publication date:
2011

Performance of diamond-like carbon-protected rubber under cyclic friction. II. Influence of substrate viscoelasticity on the friction evolution

D. Martinez-Martinez,[a] J. P. van der Pal, Y. T. Pei, and J. Th. M. De Hosson
Materials innovation institute M2i, Department of Applied Physics, University of Groningen, Nijenborgh 4, 9747 AG Groningen, Netherlands

(Received 29 June 2011; accepted 29 October 2011; published online 20 December 2011)

In this paper, the influence of the mechanical properties of rubber substrate on frictional behavior of DLC-protected rubber is studied by numerical methods. The viscoelastic contribution to the friction during a tribotest was simulated according to a "mattress" approach composed by Voigt or standard linear solid units. The latter approach demonstrated more accurate predictions. In both cases, the results show an increase of the contact depth, which is in agreement with the experimental observations. The simulations also show a progressive reduction of the viscoelastic contribution of the coefficient of friction (CoF) with the number of laps due to the elongation of the front part of the contact area. This prediction does not agree with the experimentally observed increase of CoF, and suggests a dominant contribution of the adhesive component to the friction under real conditions.
 [doi:10.1063/1.3665445]

I. INTRODUCTION

In previous papers,[1–5] we have investigated the application of flexible diamond-like carbon (DLC) films as optimal protective coating for rubbers used as seals in ball bearings. The application of the DLC film reduced the coefficient of friction (CoF) by reduction of the adhesive interaction between the rubber and its counterpart. In a previous communication,[6] we have evaluated the mechanical properties of rubber by creep experiments using the same geometry and load used in the tribotest conditions. The data were fitted to a double-Voigt model, and also used to predict the depth evolution of the ball during the tribotest. However, that approach was too simplistic to simulate the frictional behavior during the tribotest.

The aim of this work is to study the influence of the properties of the substrate on the coefficient of friction (CoF) of DLC-protected rubbers under real tribotests. To do that, two models with a different degree of complexity are evaluated: a Voigt model, and a more complex standard linear solid (SLS) model.

II. RESULTS AND DISCUSSION

A. Simulation of the frictional behavior during a tribotest using a Voigt model

Two main components can be distinguished for friction of rubber-based materials. The first one comes from the hysteresis of viscoelastic systems, which causes a difference in the energy employed by the front part of the counterpart in deforming the rubber, and the energy recovered by its rear part when relaxing. Thus, the hysteresis friction is proportional to the non-recovered energy because of the delayed response of a viscoelastic material, and therefore this effect is not present in an elastic one. The second contribution is the adhesive interaction between the rubber and the counterpart. This latter will be assumed to be zero (in fact, it is greatly minimized because of the presence of the DLC film), and it will be not considered in the present work.

We will base our approach on the work from Flom and Bueche,[7] further revised and expanded by Moore.[8] First, a Voigt model[6] is assumed to simulate the rubber behavior, and a "mattress approach" is used for calculating the contact areas. Thus, the overall behavior of the rubber is assumed to be the combination of many individual Voigt elements arranged in parallel, like springs in a mattress (see Fig. 1(a)).

The origin of the coordinates will be considered in the center of the ball. The relative motion of the ball and the rubber takes place in the x axis with a speed V. The width of track will be considered in the y axis, and the vertical displacements of the ball will vary in the z axis, taking the rubber side (bottom) as a positive direction.

The deformation Δ of rubber in a point (x, y) is:

$$\Delta = z - z_{surf}, \tag{1}$$

where z_{surf} is the vertical distance between the center of the ball and the surface of the rubber. Thus, Δ_0 would be the maximum deformation, at $x=0$, $y=0$. A Voigt element deforms according to:

$$p = k \cdot \left(g \cdot \Delta + \eta \frac{d\Delta}{dt} \right) = k \cdot g \left(\Delta + T \frac{d\Delta}{dt} \right), \tag{2}$$

where p is the pressure in a point (x, y) within the contact area, g, η, and their ratio T are the characteristics of the Voigt unit,[6] and k is a typical length dimension of the Voigt unit. The second term of Eq. (2) can be re-written as:

$$\frac{d\Delta}{dt} = \frac{d\Delta}{dx}\frac{dx}{dt} = -V\frac{d\Delta}{dx}. \tag{3}$$

[a]Author to whom correspondence should be addressed. Electronic mail: d.martinez-martinez@m2i.nl.

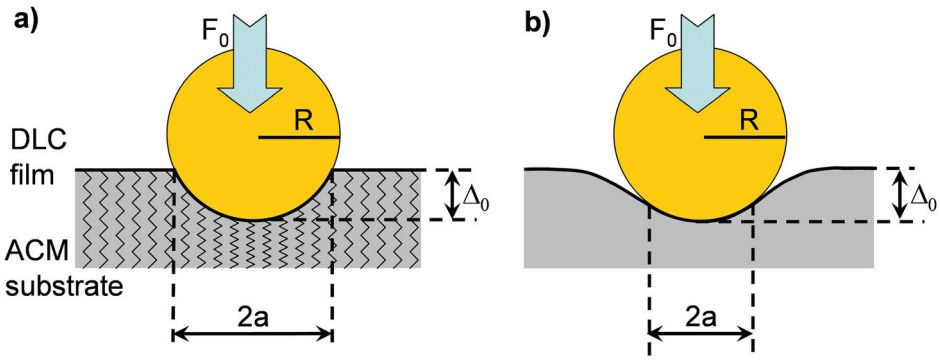

FIG. 1. (Color online) Sketches of the deformation of the rubber under spherical indentation assuming a "mattress approach" (a), and a Hertzian contact (b).

The contact area can be calculated according to the following requirement for the applied load (F_0):

$$F_0 = \int_{\text{contact area}} p dx dy, \tag{4}$$

and then, the CoF can be calculated from the momentum of the lateral force:

$$\text{CoF} = \frac{\int_{\text{contact area}} p x dx dy}{R \cdot F_0}. \tag{5}$$

The main objective of the simulation is, therefore, the calculation of the contact area using Eq. (19). In the previous analysis,[7,8] only the first pass of the ball on the rubber was considered. Although they provide valuable information about the effect of material parameters and test conditions, no information was given about the evolution of the CoF with time (i.e., in the case of consecutive laps). This treatment will be considered here, and therefore the limits of the contact area need to be revised accordingly.

The difference between the first cycle and the subsequent ones lies on the degree of deformation of the rubber in front of the ball (cf. Fig. 2). During the first cycle, the ball faces a non-deformed rubber, while in the next cycles the rubber may be not totally recovered, i.e., it has already a deformation Δz (see Fig. 2(b)); a_x and x_0 are defined as the dimensions of the contact area in the positive and negative sides of the x axis, i.e., where the ball faces the rubber and the opposite, respectively. Because of the delayed recovery of the rubber, $a_x \geq |x_0|$. In contrast, the dimensions of the contact area on the y axis are symmetric, and are represented by a_y.

The limits of the front part of the contact area can be identified through three points on the boundary of the contact between the ball and the rubber. From plane yz (see Fig. 2(a)) the points $(0, a_y, z_{surf})$ and its symmetric $(0, -a_y, z_{surf})$ can be identified, whereas $(a_x, 0, z_{surf} + \Delta z)$ is found from plane xz (see Fig. 2(b)). The plane connecting these points can be defined according the following expression:

$$z = \frac{\Delta z}{a_x} x + z_{surf}. \tag{6}$$

The distance between the center of the ball and the surface of the undeformed rubber is (cf. Figs. 2(a) and 2(b)):

$$z_{surf} = \sqrt{R^2 - a_y^2} = \sqrt{R^2 - a_x^2} - \Delta z. \tag{7}$$

The expression (7) allows calculating the relationship between a_x and a_y depending on Δz:

$$a_y = \sqrt{R^2 - \left(\sqrt{R^2 - a_x^2} - \Delta z\right)^2}. \tag{8}$$

The position of any point of the rubber in contact with the sphere is defined by its equation:

$$z = \sqrt{R^2 - x^2 - y^2}. \tag{9}$$

Thus, by combination of Eqs. (6), (7), and (9) (intersection between sphere and plane), we can arrive to an equation limiting the front part of the contact area only depending on parameter a_x:

$$y = \sqrt{R^2 - x^2 - \left(\Delta z\left(\frac{x}{a_x} - 1\right) + \sqrt{R^2 - a_x^2}\right)^2}. \tag{10}$$

Particular cases of this equation can be considered to evaluate its accuracy. For instance, at $x = 0$, $y = a_y$ (cf. Eq. (8)),

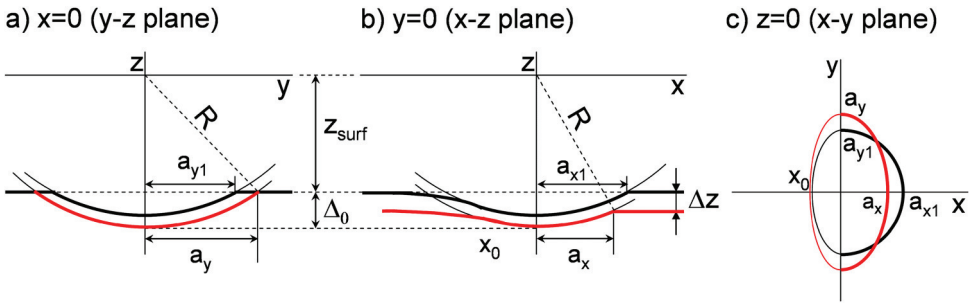

FIG. 2. (Color online) Scheme of the contact area between the ball and the substrate for a given cycle. The situation during the first cycle is also depicted in black for comparative purposes (a_{x1}, a_{y1}): (a) $x = 0$ (yz plane), (b) $y = 0$ (xz plane), and (c) $z = 0$ (xy plane).

and at $x = a_x$, $y = 0$. Finally, it is interesting to check the validity on the first cycle, i.e., $\Delta z = 0$. In this case, Eq. (10) becomes the equation of a circumference:

$$y = \sqrt{a_x^2 - x^2}. \tag{11}$$

Thus, it is clear that the front part of the contact area is symmetric (i.e., $a_x = a_y$) in case of a not previously deformed substrate (i.e., $\Delta z = 0$, cf. Eq. (8)). In contrast, after the first cycle, this symmetry may be broken, and the contact area reduced in the x axis and elongated in the y axis (see Fig. 2(c)). In previous works,[7,8] the asymmetry of the contact area was only described in terms of front−back (i.e., $a_x \geq |x_0|$) caused by the delayed response of the substrate. However, a second source of asymmetry of the contact area may appear after the first cycle (elongation), which is only canceled in case of full recovery of the rubber during the rest of the cycle.

The deformation for any given point of the rubber can be calculated according to Eqs. (1), (7), and (9):

$$\Delta = \sqrt{R^2 - x^2 - y^2} - \sqrt{R^2 - a_x^2} + \Delta z, \tag{12a}$$

which can be simplified using the Taylor approximation to:

$$\Delta = \frac{1}{2R}\left(a_x^2 - x^2 - y^2\right) + \Delta z, \tag{12b}$$

therefore, we can re-write Eq. (2) considering Eqs. (3) and (12a):

$$p = k \cdot g \cdot \left[\sqrt{R^2 - x^2 - y^2} - \sqrt{R^2 - a_x^2} + \Delta z + \frac{T \cdot V \cdot x}{\sqrt{R^2 - x^2 - y^2}}\right]. \tag{13}$$

The value of k can be obtained by the combination of Eqs. (4) and (13), after its particularization to static ($V = 0$) and elastic conditions (i.e., $a_x = a_y = a$). Thus, if the first cycle is considered ($\Delta z = 0$) and the rubber is incompressible and elastic ($\nu = 0.5$, $\eta = 0$), an approximate solution for Eq. (4) can be obtained using a Fourier expansion for the square roots, because x, y, and a are much lower than R;[7,8]

$$F_0 \approx k\frac{\pi \cdot G \cdot a^4}{2R}, \tag{14}$$

in addition, the equation of Herztian contact is:

$$F_0 = \frac{8}{3}\frac{2G}{R}a^3, \tag{15}$$

and by comparison of Eqs. (14) and (15), we arrive at:[7,8]

$$k = \frac{32}{3\pi \cdot a}, \tag{16}$$

which has the dimensions of inverse length, as expected. The calculation of the limits of the back part of the contact area is performed by finding the points verifying that $p = 0$ in Eq. (13). Approximated equations describing these limits can be found,[7,8] but in the present work these points have been identified numerically.

A flow chart indicating the different processes taking place during simulation is depicted in Fig. 3. The input parameters are the material properties (g, η), test conditions (load (F_0), speed (V), ball radius (R), test radius, and number of laps), and two operational parameters (error allowed during estimation of F_0 and the mesh size to discretize the contact area). For each lap, several values of a_x are evaluated, which already define the limits of the front part of the contact area (cf. Eq. (10)). The back limits of the contact area are found by identifying the points (x, y) canceling Eq. (13). The limits of the contact area are considered correct when the sum of the forces evaluated in the mesh equals the applied force within the prescribed error (typically less than 0.1%). At that moment, the output parameters are obtained, such as distribution of pressures and friction coefficient, etc. Afterward, a new value of Δz is calculated at point x_0 by the recovery procedure described in Ref. 6 considering only one Voigt unit. The program finishes when the total number of laps (n_{laps}) is reached.

Figure 4 shows the predictions of the model for the same conditions as in our tribotests. Because the present model is developed for a single Voigt unit, the values of $g = [(1/g_1) + (1/g_2)]^{-1}$ and $\eta = \eta_2$ were used. The results are depicted in Fig. 4(a). It can be seen that the depth increases with the number of laps, in agreement with previous results. However, the CoF shows a clear reduction in the same interval, which can be correlated with the elongation of the front part of the contact area as a result of the decrease of a_x and increase of a_y. However, the viscoelastic contribution to the CoF is never canceled, because there is a certain recovery during the fraction of the lap without contact between the ball and the point of the rubber under study. In addition, the contact area increases progressively, which is not evident considering its aforementioned elongation. The combination of both results suggests that the experimentally observed increase of CoF with the number of laps is not caused by the viscoelastic contribution to friction, but by a larger adhesive contribution originated by a larger contact area.

Nevertheless, the values of contact depth are much smaller than observed previously,[6] which is a consequence of the model used. First, the Voigt simulation unit is too

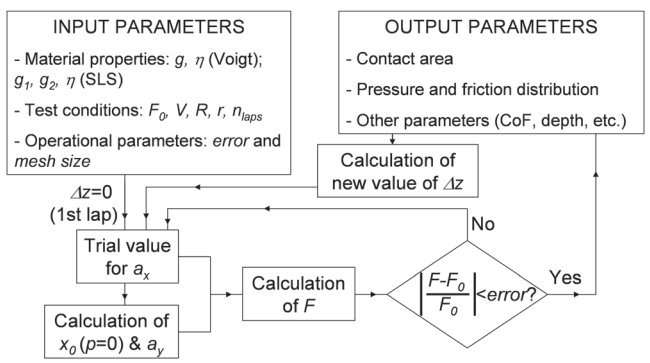

FIG. 3. Flow chart indicating the operation during simulation.

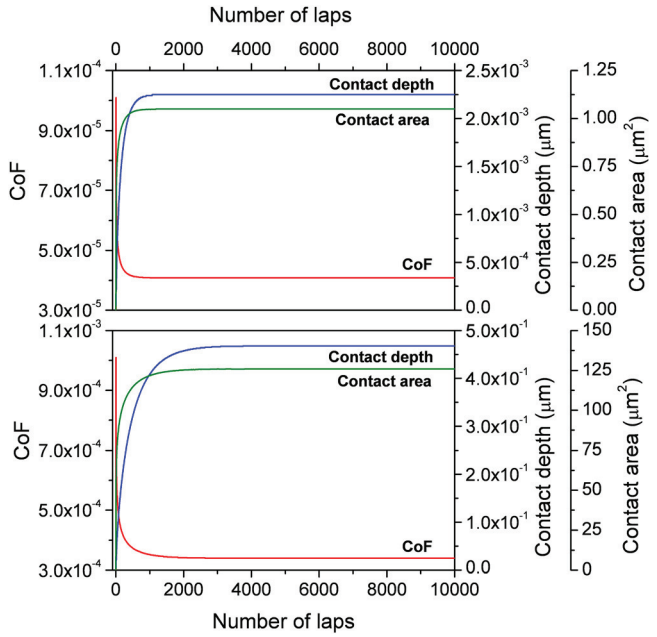

FIG. 4. (Color online) Results of the simulation for ACM rubber using the test conditions used experimentally. (a) $g = 0{,}15$ GPa and $\eta = 20{,}5$ GPa·s, and (b) $g = 0{,}15$ MPa and $\eta = 20{,}5$ MPa·s.

simple to account, even qualitatively, for a realistic viscoelastic behavior, as will be discussed afterward. Second, the contact is approached by a non-Hertzian model; the form of Eq. (2) implies that the pressure is proportional to displacement, whereas Hertzian theory requires that pressure is proportional to the square root of the displacement.[8] In addition, the mattress approach assumes no shear interaction between the different Voigt units, and therefore the surface does not depress ahead of the roller.[9] Moreover, the value of k is adjusted in steady conditions to fit with the Hertzian value of the contact area, not of the contact depth (see Eqs. (14) and (16)). Therefore, the values of contact depth can be underestimated (see Fig. 1). Thus, lower values of the material properties are needed to reproduce the observed values of depth, as can be seen in Fig. 4(b). This modification leads to higher values of CoF and contact area than in the previous case, as expected. In any case, the trends of all the monitored parameters (CoF, contact area, contact depth, etc.) with the number of laps are the same as in the previous case.

The influence of the test speed (or frequency) is very interesting for viscoelastic materials, because their properties depend on that parameter. The time of travel through the semicontact length is:

$$t = \frac{a_x}{V}. \tag{17}$$

The ratio of this time and the relaxation time of the Voigt (T) unit is a non-dimensional parameter called the "Deborah number" (ζ_1):

$$\zeta_1 = \frac{VT}{a_x}. \tag{18a}$$

In a similar manner, a second non-dimensional parameter ζ_2 can be defined to compare the rubber relaxation time and the time needed to cover a full tribotest lap:

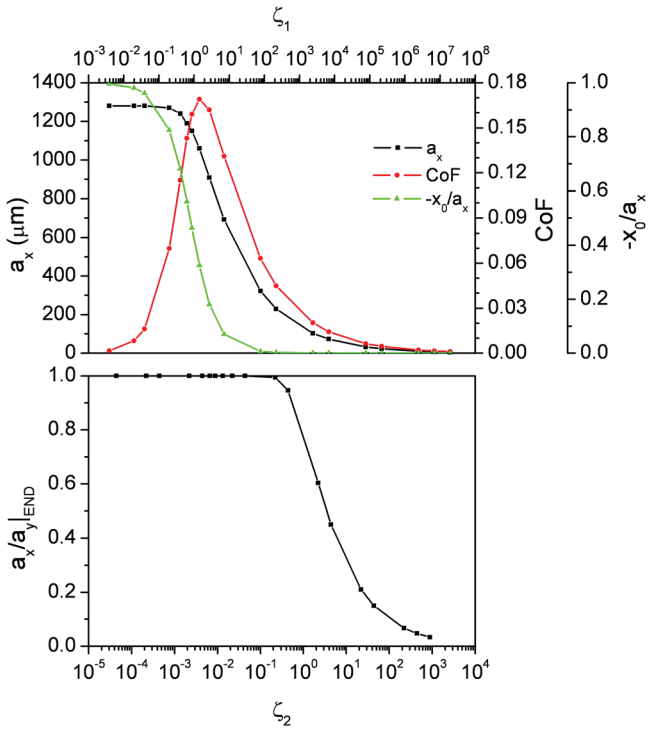

FIG. 5. (Color online) Influence of the frequency on different properties of the contact area for a Voigt model with $g = 0{,}5$ MPa and $\eta = 250$ MPa·s. (a) CoF, and size and asymmetry of the contact area in the x axis, and (b) elongation of the contact area.

$$\zeta_2 = \frac{VT}{2\pi r}. \tag{18b}$$

Figure 5 shows the dependence of several parameters with ζ_1 and ζ_2. It can be seen that the contact area shows a strong reduction and a peak of CoF is observed at $\zeta_1 \sim 1$, in agreement with previous results.[9] It can be seen that the asymmetry ratio a_y/a_x starts to increase at $\zeta_2 \sim 1$, in agreement with the lower time given for recovery. In addition, the other asymmetry ratio $-x_0/a_x$ decreases to zero at high values of ζ_1. This is, in fact, the main qualitative disagreement of this model with the experimental results, which show a maximum asymmetry at a certain ζ_1, and a recovery of the circular contact area at high speeds.[8] This disagreement is caused by the inherent simplicity of the Voigt model used, which also is a problem in case of a Maxwell model[10] (see Table I). It can be demonstrated that the ratio $-x_0/a_x$ is correlated univocally with the ratio between the loss and storage compliances (C''/C') of the viscoelastic material.[8] This latter ratio is typically referred as tanδ, being δ the angle retardation between C'' and C'. Therefore, for $\delta = 0$ we get $-x_0/a_x = 1$ (i.e., circular contact area for elastic conditions), and for $\delta = \pi/2$ we get $x_0/a_x = 0$ (i.e., semicircular contact area for

TABLE I. Characteristics of different viscoelastic models.

Model	$p(x = a_x)$	*CoF* vs V	$-x_0/a_x$ vs V	tanδ vs ω
Voigt	High	Peak	Decreases (1 to 0)	Grows
Maxwell	Zero	No peak	Grows (0 to 1)	Decreases
SLS	Zero	Peak	Peak	Peak

viscous conditions). In real materials, tanδ shows a maximum at a certain frequency. However, this is not the case for a Voigt model, which has the following linear dependence with the frequency:

$$\tan\delta = \omega T = \zeta_1, \tag{19}$$

considering that the reciprocal of Eq. (17) has dimensions of frequency.[8] As a result, the peak of tanδ is missing, and therefore no maximum for asymmetry is observed. A solution for this inconvenience is using a more complex model for simulation, as it will be shown for a SLS in the next section; in this case, tanδ shows a maximum with frequency, because:[8]

$$\tan\delta = \frac{\omega\dfrac{\eta}{g_2}}{1+\dfrac{g_2}{g_1}\left(1+\left(\omega\dfrac{\eta}{g_2}\right)^2\right)}, \tag{20}$$

However, the Voigt model reproduces very well the reduction of the contact area experimentally observed with the speed, because C' reproduces the stiffening of the rubber with the test frequency:[8]

$$C' = \frac{1}{g\left(1+(\omega T)^2\right)}, \tag{21}$$

In addition, the Voigt model is able to predict a maximum of CoF at a certain speed, which is therefore not connected with a maximum asymmetry of the contact area. In fact, the values of CoF at high speeds are probably overestimated, because the back part of the contact area (which reduces the CoF) is predicted to disappear ($x_0/a_x = 0$).

B. Simulation of the frictional behavior during a tribotest using a standard linear solid

The previous model can be much improved by its modification of the inclusion of a spring in series with the Voigt unit, becoming a SLS.[6] To do that, an expression equivalent to Eq. (13) has to be found. For a SLS, the relationship between stress and strain is described by:[8]

$$\frac{dp}{dt}+\frac{g_1+g_2}{\eta}p = k\left(g_1\frac{d\Delta}{dt}+\frac{g_1g_2}{\eta}\Delta\right), \tag{22}$$

which corresponds to Eq. (2) in the Voigt model. The solution of this ordinary differential equation is:

$$p(t) = k\left[\frac{g_1g_2}{g_1+g_2}\Delta+\frac{g_1^2\eta^2}{(g_1+g_2)^3}\frac{V}{R}\times\left(V+\frac{g_1+g_2}{\eta}(a_x(y)-VT)\right)\right] + C\exp\left(-\frac{g_1+g_2}{\eta}t\right), \tag{23}$$

where C is an integration constant, whose value can be obtained considering that, at $t=0$, $p=0$ if $\Delta=0$. Including also the geometrical considerations (Eq. (2b)), Eq. (23) can be re-written as:

$$p(x,y) = \frac{g_1}{g_1+g_2}\frac{k}{2R}\left[g_2\left(a_x^2-x^2-y^2+2R\Delta z\right) -2g_1V^2T_1^2\left\{\left[1+\frac{a_x(y)}{VT_1}\right]\cdot\left[\exp\left(-\frac{a_x(y)-x}{VT_1}\right)-1\right] +\frac{a_x(y)-x}{VT_1}\right\}\right] \tag{24}$$

where

$$T_1 = \frac{\eta}{g_1+g_2}, \tag{25}$$

and $a_x(y)$ represents the x coordinate on the front part of the contact area for an abscissa y (i.e., $a_x(y=0)=a_x$). This parameter can be obtained from Eq. (10), after using the Taylor approximation for the square roots as:

$$a_x(y) = \sqrt{\left(\frac{R\Delta z}{a_x}\right)^2+2R\Delta z+\left(a_x^2-y^2\right)}-\frac{R\Delta z}{a_x}. \tag{26}$$

The particularization of Eqs. (24)–(26) to a cylindrical geometry leads to the expression obtained by Johnson using the superposition principle approach.[9] Figure 6 shows the pressure profiles in the x axis according to Eq. (39) for SLS arrangements with different values of g_1. It can be seen that at values of g_1 comparable to g_2, the contact area is large and the maximum contact pressures are reduced. The increase of the ratio g_1/g_2 makes the isolated spring of the SLS stiffer, and therefore closer to a pure Voigt system. Thus, the pressure profiles at g_1/g_2 ratios larger than 100 follows the profile observed for a Voigt unit alone very well, indicating the correctness of Eq. (24). In fact, another important advantage can be seen when comparing with the Voigt profile, which predicts that pressure does not go to zero at $x=a_x$. This is caused by the right term in Eq. (13), where speed plays a

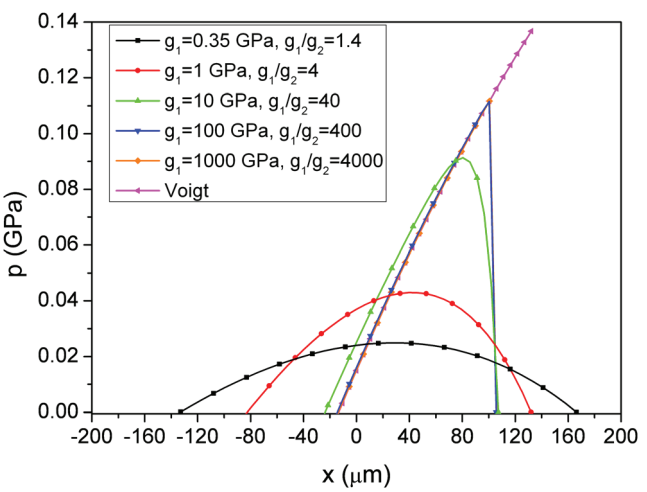

FIG. 6. (Color online) Influence of the strength of the isolated spring (g_1) on the pressure profiles along the x axis for different SLS models. The profile of an isolated Voigt model with the same characteristics as the Voigt unit in the SLS is also displayed for comparison purposes.

role, and it is a direct consequence of the problems of the Voigt model to predict the creep behavior at zero deformation times. Thus, this characteristic makes the SLS model even a better option to simulate the rubber behavior in tribotest conditions (see Table I).

To account for the rubber relaxation during the unloading part of each lap, the same function as in the previous case can be used, because this process is just controlled by the Voigt unit in the SLS, whose relaxation time is:

$$T_2 = \frac{\eta}{g_2}. \tag{27}$$

Thus, the definition of the two non-dimensional parameters for a standard linear solid has to be:

$$\zeta_1 = \frac{VT_1}{a_x}, \tag{28a}$$

$$\zeta_2 = \frac{VT_2}{2\pi r}, \tag{28b}$$

because T_1 and T_2 control the rubber response during loading and its further relaxation, respectively. The influence of both parameters in the rubber behavior is depicted in Fig. 7 in the left and right columns, respectively. Because the g_1/g_2 ratio defines the degree of elasticity of the whole system, two sets of data with different ratios have been calculated for comparison purposes, keeping the sum $g_1 + g_2$ constant to make T_1 invariant (see Eq. (25)). Thus, the experimentally observed[6] $g_1/g_2 = 1.4$, and its ten multiple, $g_1/g_2 = 14$, have been used. Figure 7(a) shows the evolution of the asymmetry of the contact area. As expected, the SLS model is able to reproduce the symmetry recovery of the contact area at high speeds (i.e., at high values of ζ_1). This is of particular importance, because the experimental tribotests are carried out in those conditions, and the results are totally different than the ones obtained from the Voigt model (cf. Fig. 5(a)). In addition, it can be seen that the maximum asymmetry is larger for the less elastic model (higher g_1/g_2). This one also shows a larger CoF peak (Fig. 7(c)), and larger variation of the contact area (Fig. 7(e)), in agreement with a stronger viscous influence. In addition to that, a displacement of the peaks to lower values of ζ_1 can be appreciated, which is also caused by the different viscoelastic properties of the material; Eq. (20) can be re-written as:

$$\tan\delta = \frac{\zeta_1 \dfrac{g_1}{g_2}}{1 + \zeta_1^2\left(1 + \dfrac{g_1}{g_2}\right)}. \tag{29}$$

This function is depicted for both cases in Fig. 7(f). It can be seen that the tanδ peak is displaced to the left and its intensity is increased. By the comparison of this plot with the ones above, the influence of the macroscopic properties of the rubber on its behavior during tribological tests is clear. It has to be noticed that these effects are centered around $\zeta_1 \sim 1$ only for the cases verifying that $g_1/g_2 \ll 1$, because the maxima of tanδ are located at:

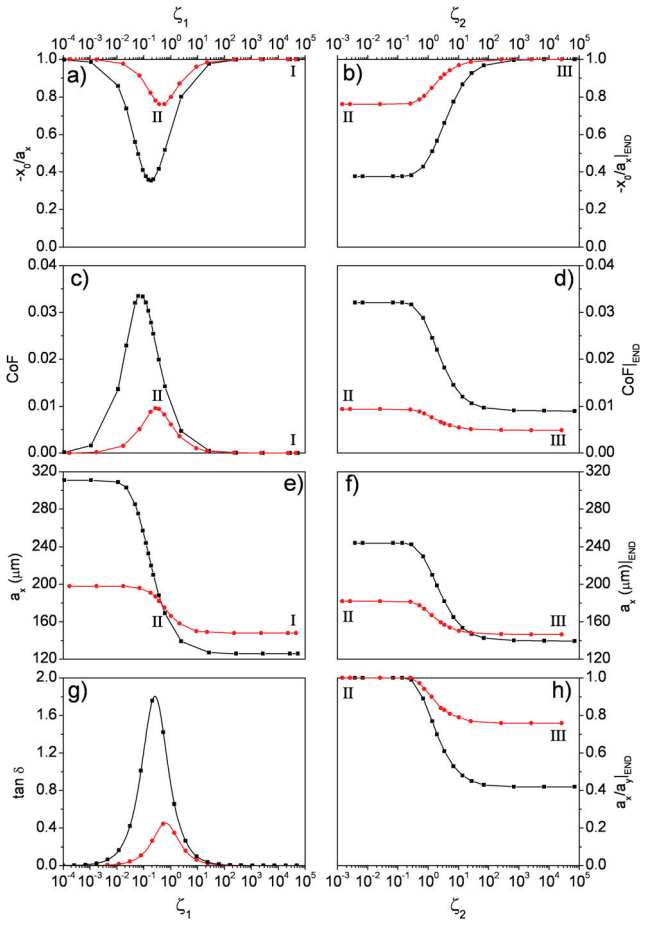

FIG. 7. (Color online) Influence of tribotest speed (related to ζ_1) and frequency (related to ζ_2) in different relevant parameters: asymmetry in the x axis (a, b); CoF (c, d); size of the contact area in the x axis (e, f); tanδ (g); elongation of the contact area (h). Left column: influence of ζ_1. Right column: influence of ζ_2 in the case of $\zeta_1 \sim 1$ on the steady-state condition of the tribotest. Results for two different SLS models with different degrees of elasticity (different g_1/g_2 ratio but same T_1) are shown: (circles) $g_1/g_2 = 1.4$, (squares) $g_1/g_2 = 14$. Situations I, II, and III are detailed in Fig. 8.

$$\zeta_1(\tan\delta_{\max}) = \sqrt{\frac{1}{1 + \dfrac{g_1}{g_2}}}. \tag{30}$$

Nevertheless, in all of these cases, there was no evolution during the tribotest, i.e., the values of all the parameters under study were the same after the first and the final lap. In addition, in none of these cases was there any elongation of the contact area. This lack of variations is caused by a combination of two factors, as will be explained now.

The right column of Fig. 7 shows the influence of ζ_2 on several parameters recorded at the end of the tribotest. This study has been carried out for both samples at the speed conditions that showed the maximum asymmetry of the contact area. To keep ζ_1 constant, ζ_2 has been varied by modifications of the track radius (i.e., reduction of the rubber recovery by reducing the track length, see Eq. (28)). It can be seen that for low values of ζ_2, all of the parameters under study are constant, and equal to the values observed at the first cycle (i.e., no variations are seen during the tribotests). The elongation parameter $a_x/a_y = 1$ (cf. Fig. 7(h)). However, at

$\zeta_2 \sim 1$, some elongation begins to appear, and the other parameters start to be modified. The CoF is reduced, in agreement with the results observed in the Voigt model (cf. Fig. 4), and the same is seen for the size of the semicontact area. Further, the symmetry of the contact ($-x_0/a_x$) starts to increase. It is worth noting that larger variations are observed again for the less elastic sample (larger g_1/g_2). All the parameters reach a new steady state at high values of ζ_2, which is caused because the ratio $-x_0/a_x$ reaches its limit. In other words, the maximum evolution of the different parameters during a tribotest is limited by the symmetry of the contact area. As a consequence, to see any modification caused by the elongation of the contact area, the system has to be tested in viscoelastic conditions (i.e., in the region of the peak in tanδ, otherwise the rubber behaves elastically).

That explains why such elongation was not observed in the previous analysis of ζ_1, because at high values of ζ_1, the contact area was already symmetric. In contrast, at values of ζ_1 where the asymmetry was present, the values of ζ_2 were too low to see the elongation effect, because the time to recover the previous deformation was too long. Thus, the elongation of the contact area does take place only if the asymmetry condition is given (i.e., which is described in Eq. (30)) and not enough time is given to the rubber to relax after each pass (i.e., $\zeta_2 \geq 1$). In the case of the Voigt model, variations were observed at high values of ζ_2 (cf. Fig. 5(b)), because this model predicts asymmetry also in the case of $\zeta_1 \gg 1$ (see Table I).

Some examples of the contact pressure and CoF distributions within the contact area are depicted in Fig. 8 for the sample with $g_1/g_2 = 1.4$ for the three situations labeled as I, II, and III in Fig. 7. The plots on the top represent the pressure distributions within the contact area, while the bottom ones represent the distribution of CoF. It has to be noted that the overall contact pressure is the average of the contact pressure map, while the total CoF is the sum of all the values of CoFs. In each case, the distribution at the end and at the beginning of the test ($\Delta z = 0$) are depicted for negative and positive values of the y axis, respectively. The materials properties obtained for 1 N have been used[6] (i.e., $g_1 = 0.35$, $g_2 = 0.25$, and $\eta = 20.5$ GPa·s). The results obtained in Fig. 7(a) correspond to the tribotest conditions used experimentally.[6] It can be seen that under such conditions ($\zeta_1 \gg 1$), the model predicts a circular contact area and an overall zero CoF. In this case, the ball depth reaches 3.63 μm, in good agreement with the experimentally observed values.[6] In addition, it can be seen that the initial and final geometries are the same, which indicates no elongation of the contact area and no evolution of any of the parameters during the tribotest. This result does not agree with what was experimentally observed, and it is probably caused by the low capability of creep measurements to evaluate mechanical properties of the rubber at high deformation frequencies. Figure 7(b) shows the appearance of contact asymmetry at lower values of ζ_1 (i.e., lower test speeds). It can be seen that the point of maximum pressure is displaced from the center, and also that the equilibrium between the CoF observed at the front and the back of the contact area is broken. However, it has to be clarified that the value of ζ_1 showing larger asymmetry of the contact area does not correspond exactly with

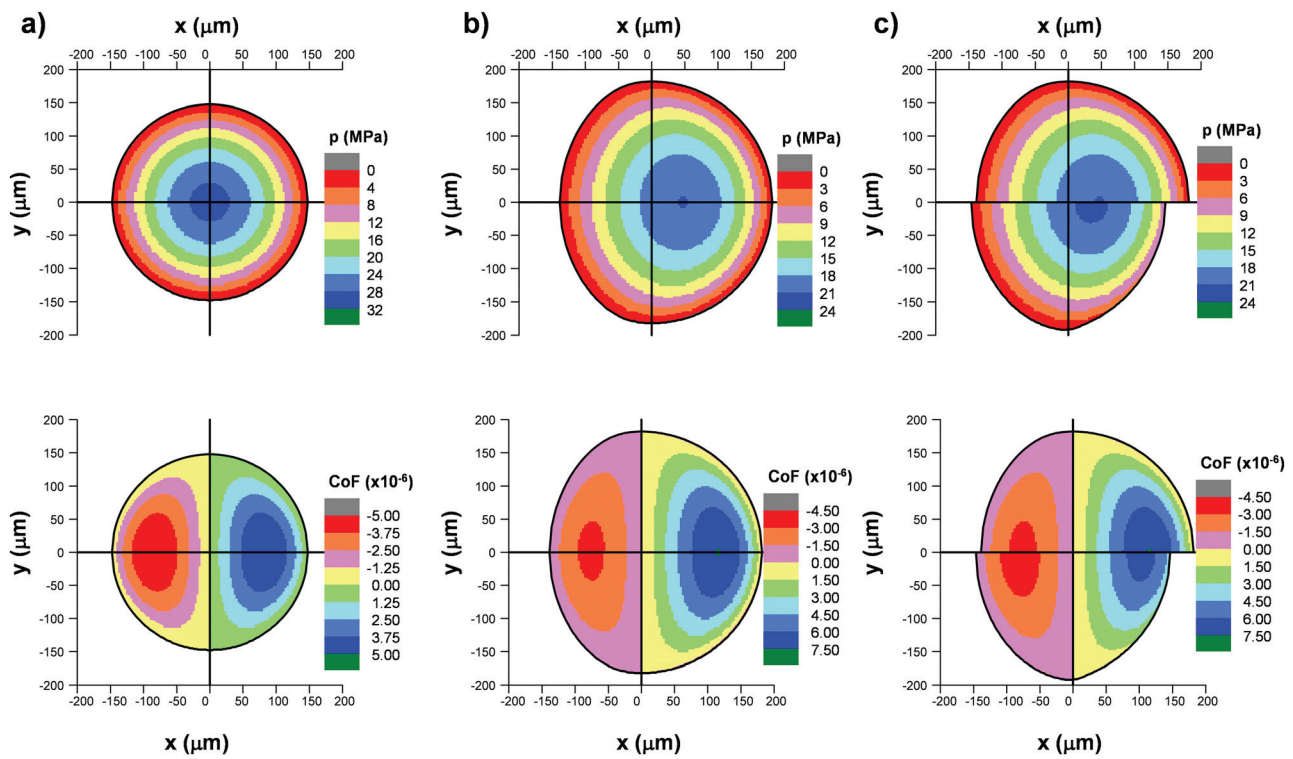

FIG. 8. (Color online) Distribution of contact pressure (top) and CoF (bottom) within the contact area for a SLS model with the $g_1 = 0.35$ GPa, $g_2 = 0.25$ GPa, and $\eta = 20.5$ GPa·s at the conditions labeled as I, II, and III in Fig. 7. The distributions at the beginning and at the end of the test are depicted on each plot on the positive and negative regions of the y axis, respectively: (a) situation I, (b) situation II, and (c) situation III.

the maximum CoF (cf. Figs. 7(a) and 7(c)), because of the variations of the size of the contact area in this range (see Fig. 7(e)). No elongation of the contact area is observed because of the low value of ζ_2. In contrast, a clear modification can be detected in Fig. 7(c), although the geometries of the first lap are the same as in Fig. 7(b) (of course, the modification of the tribotest radius does not influence the first lap). At the end of the test, lower positive values of CoF are observed, while larger negative values are seen. This fact, together with the increase of the $-x_0/a_x$ ratio, leads to the reduction of CoF (cf. Figs. 7(b) and 7(d)). In addition, it is worth noting that the pressure and CoF are not canceled in the limits of the front part of the contact area at the end of this test. This is caused by the non-recovered deformation from the previous lap, which makes certain parts of the deformed rubber to be not in contact with the ball (cf. Fig. 2). In other words, the rubber is deformed beyond the contact area between the rubber and the ball because of the presence of previous deformations. In contrast, in all of the other depicted cases, the CoF and the pressure equal zero in the limits of the contact area, which is not what is observed in the case of a Voigt model.

Figure 9 depicts the images of the counterpart after tribotests carried out on four types of ion-etched rubbers: flourocarbon rubber (FKM), acrylic rubber (alkyl acrylate copolymer, ACM), hydrogenated nitrile butadiene rubber (HNBR), and nitrile butadiene rubber (NBR). The ion-etching treatment is preferred to the protection with a DLC film, because the adhesion between the counterpart and the tested specimens is much lower in the latter case, and the shape of the contact area cannot be identified. Further information about the preparation and properties of these samples can be found elsewhere.[11] In all cases, the shape of the contact area is similar to those depicted in Figs. 8(b) and 8(c). The $-x_0/a_x$ ratios are lower than 1, reflecting a viscoelastic condition. Moreover, the a_x/a_y ratios are also lower than 1, in agreement with the elongation predicted by the model. In fact, the comparison of different measurements showed that larger elongations were obtained when the parameter $-x_0/a_x$ was closer to 1. This result agrees with the trends observed in Figs. 7(b) and 7(h).

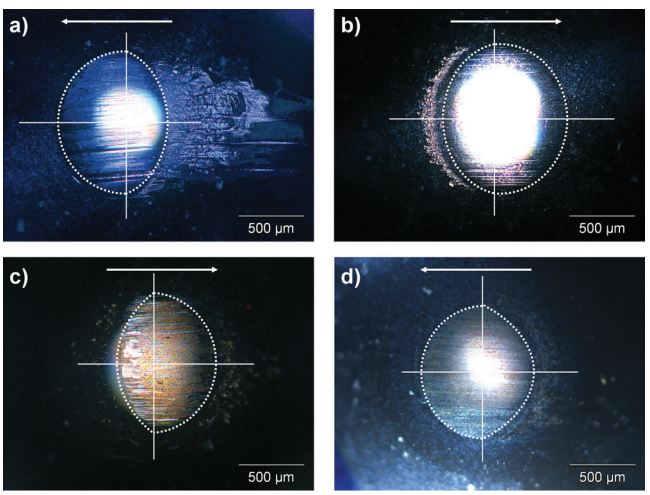

FIG. 9. (Color online) Images of the spherical counterpart after tribotests performed in different rubbers: (a) ACM, (b) HNBR, (c) FKM, and (d) NBR. The limits of the contact area have been highlighted by dashed lines. The direction of movement of the ball during the tribotest is indicated by arrows.

Although the qualitative predictions of the model appear to be correct, still some disagreements can be identified. First, the dimensions of the contact area do not fit exactly with those experimentally observed. Second, the simulation fails to predict the modifications of the contact area at the experimental test conditions (see Fig. 7, point I and Fig. 8(a)). To get semiquantitative results, more sophisticated measurements and models need to be used. The experimental evaluation of mechanical properties has to be carried out at higher frequencies, to introduce information on the model about its response at very low interaction times. Therefore, dynamic mechanical thermal analysis (DMTA) measurements can be more adequate. As a consequence, the fitting model will need to increase its complexity to adjust several frequencies. In addition, a Hertzian approach would be preferred to enhance the accuracy of the simulations. All of these improvements will be covered in a forthcoming paper.

III. CONCLUSIONS

The evolution of the viscoelastic component of friction of DLC-coated rubbers during tribotests was studied qualitatively with a simple Voigt and the more complex standard linear solid (SLS) models using a mattress approach. The SLS produced better results, showing the proper evolution of the contact asymmetry with the test frequency and avoiding the problem of non-zero pressure in the front limits of the contact area. An equation for the evolution of the contact with the number of laps area was proposed, which allows simulating the frictional behavior in a real tribotest. It predicts the elongation of the front part of the contact area if the previous deformation of the rubber is not recovered, which agrees with the experimental observations. The results of the simulations show that this elongation only appears provided the contact area is not fully symmetric. Under these conditions, a reduction of the viscoelastic contribution to the CoF with the number of laps is observed. All of these effects are greater in the case of a less elastic system. Therefore, the experimentally observed increase of CoF is probably caused by a higher contribution of the adhesive CoF, in agreement with the predicted increase of the contact area.

ACKNOWLEDGMENTS

This research was carried out under Project No. MC7.06247 in the framework of the Research Program of the Materials Innovation Institute M2i (www.m2i.nl), Delft, the Netherlands. Dr. X.B. Zhou of the SKF Engineering & Research Center in Nieuwegein, the Netherlands is thanked for his valuable input.

[1]M. Schenkel, D. Martinez-Martinez, Y. T. Pei, and J. T. M. De Hosson, Surf. Coat. Technol. **205**, 4838 (2011).
[2]D. Martinez-Martinez, M. Schenkel, Y. T. Pei, and J. T. M. De Hosson, Thin Solid Films **519**, 2213 (2011).

[3]D. Martinez-Martinez, M. Schenkel, Y. T. Pei, and J. T. M. De Hosson, Surf. Coat. Technol. **205**, S75 (2011).
[4]Y. T. Pei, X. L. Bui, and J. T. M. De Hosson, Scr. Mater. **63**, 649 (2010).
[5]X. L. Bui, Y. T. Pei, E. D. G. Mulder, and J. T. M. De Hosson, Surf. Coat. Technol. **203**, 1964 (2009).
[6]D. Martinez-Martinez, J. P. van der Pal, Y. T. Pei, and J. T. M. De Hosson, J. Appl. Phys. 110, 124906 (2011).
[7]D. G. Flom and A. M. Bueche, J. Appl. Phys. **30**, 1725 (1959).
[8]D. F. Moore, *The Friction and Lubrication of Elastomers* (Pergamon, New York, 1972).
[9]K. L. Johnson, *Contact Mechanics* (Cambridge University Press, Cambridge, 1987).
[10]W. D. May, E. L. Morris, and D. Atack, J. Appl. Phys. **30**, 1713 (1959).
[11]D. J. Wolthuizen, D. Martinez-Martinez, Y. T. Pei, and J. T. M. De Hosson, "Influence of plasma etching on the tribological performance of rubbers," Tribol. Lett. (submitted).